Journal of Magnetic Resonance **143,** 79–87 (2000)
doi:10.1006/jmre.1999.1956, available online at http://www.idealibrary.com on IDEAL®

A New Class of Contrast Agents for MRI Based on Proton Chemical Exchange Dependent Saturation Transfer (CEST)

K. M. Ward,[1] A. H. Aletras, and R. S. Balaban[2]

Laboratory of Cardiac Energetics, National Heart, Lung, and Blood Institute, Building 10, Room B1D-416, National Institutes of Health, Bethesda, Maryland 20892-1061

Received June 16, 1999; revised October 13, 1999

It has been previously shown that intrinsic metabolites can be imaged based on their water proton exchange rates using saturation transfer techniques. The goal of this study was to identify an appropriate chemical exchange site that could be developed for use as an exogenous chemical exchange dependent saturation transfer (CEST) contrast agent under physiological conditions. These agents would function by reducing the water proton signal through a chemical exchange site on the agent via saturation transfer. The ideal chemical exchange site would have a large chemical shift from water. This permits a high exchange rate without approaching the fast exchange limit at physiological pH (6.5–7.6) and temperature (37°C), as well as minimizing problems associated with magnetic field susceptibility. Numerous candidate chemicals (amino acids, sugars, nucleotides, heterocyclic ring chemicals) were evaluated in this preliminary study. Of these, barbituric acid and 5,6-dihydrouracil were more fully characterized with regard to pH, temperature, and concentration CEST effects. The best chemical exchange site found was the 5.33-ppm indole ring –NH site of 5-hydroxytryptophan. These data demonstrate that a CEST-based exogenous contrast agent for MRI is feasible.

Key Words: **barbiturate; sugars; polymers; spin–lattice relaxation rate; amino acids; heterocyclic chemistry; indole.**

INTRODUCTION

Exogenous contrast agents are often used to provide enhanced image contrast as well as to improve the specificity of MRI. These contrast agents generally work by altering the water proton T_1, T_2, or both parameters. The types of MRI contrast agents are quite diverse and include paramagnetic chelated metal ions (Gd-DPTA) (*1*), diamagnetic ions in combination with superparamagnetic ions (*2*), proton chemical exchange agents acting through T_2 relaxation properties (*3*), or dipolar interactions between water and the immobilized agent (*4, 5*). Metal chelates or metal particles are the most popular MRI contrast agents. The metal-based contrast agents can be restricted to low-dose applications by toxicity or T_2^* effects which can limit some applications. In addition, metal agents suffer from the drawback that, once administered, the changes in tissue parameters persist until the agent has cleared the tissue or body.

Based on these limitations, a metal-free MRI contrast agent may be desirable. Use of chemical-exchange-dependent saturation transfer (CEST) methods in combination with agents possessing a proton exchange site can provide a significant change in the magnitude of the water proton signal (see Theory), potentially providing a non-metal-based contrast mechanism. This indirect detection technique also results in a significant gain relative to specific agent concentration (*6*). In addition, the system is relatively unperturbed by the contrast agent unless the specific saturation of the exchanging site is performed, in contrast to metal-based agents. Saturation or magnetization transfer (MT) techniques are currently exploited in generating contrast based on macromolecule–water proton interactions by using a single off-resonance irradiation of the relatively small macromolecular proton pool (*7*). Proton chemical exchange between a metabolite and water interrogated with CEST generates MRI contrast based on the exchange rate and concentration of the metabolite. This has been demonstrated in phantoms (*7*) and *ex vivo* kidney preparations (*8*). These results suggested that if a molecule with appropriate chemical exchange sites was identified, then the CEST approach could provide a new class of MRI contrast agents.

The purpose of this study was to begin to find and evaluate specific chemical groups that could function as effective proton chemical exchange partners with water for use as exogenous contrast agents. Such chemical groups would have to possess appropriate proton exchange rates as well as chemical shift properties at physiological pH and temperature.

Theory

The effect of chemical exchange on the water proton signal can be estimated from the equation (*9*)

$$M_S/M_O \approx [1 - k_1 T_{1SAT}], \qquad [1]$$

[1] Present address: The CNA Corp., 4401 Ford Avenue, RM1131 Bullpen, Alexandria, VA 22302-2029.

[2] To whom correspondence should be addressed.

1090-7807/00

where M_S is the magnitude of the water proton signal during the saturation of the exchangeable protons on the metabolite of interest; M_O is the magnitude of the signal under control irradiation at the opposite frequency offset; k_1 is the pseudo first-order exchange rate constant; and T_{1SAT} is the spin–lattice relaxation time constant of water protons as measured while the exchange metabolite is saturated. In simple reactions, the pseudo first-order exchange rate constant, k_1, is the single exchange site rate constant, k_{CA} (s^{-1}), multiplied by the total number of chemical exchange sites available as determined by the mole fraction and number of exchanging protons (n) per molecule (*10*):

$$k_1 = k_{CA}[\text{Agent}][n]. \quad [2]$$

As long as k_{CA} is rapid but does not approach the fast exchange limit (see below) significant increases in the proton signal associated with metabolites with exchangeable sites can be obtained by indirect detection through the water proton signal. This concept has been exploited for the detection of ammonia and urea in phantoms and the kidney (*6, 8*). Similar indirect detection schemes have also been used with other nuclides; examples include ^{31}P NMR CEST studies between enzyme-bound and free metabolites (*11*) and ^{13}C NMR CEST studies of dissolved CO_2 and bicarbonate (*12*).

Several other factors must be considered in order to optimize a chemical compound as an exogenous contrast agent based on CEST and are discussed below.

Chemical exchange rate. The single site exchange rate constant, k_{CA}, should be as large as possible to enhance the CEST effect as described in Eq. [1]. However, it must also remain in the slow to intermediate exchange rate domain to ensure that a discrete spectral difference between water and the agent is maintained. The slow to intermediate exchange rate domain is defined as (*10*)

$$\tau_{CA}\Delta\omega_{CA} \gg 1, \quad [3]$$

where $\Delta\omega_{CA}$ is the chemical shift difference (in rad/s) between the exchange site proton and water, and τ_{CA} is the single site proton lifetime (s). The site proton lifetime is the reciprocal of the single site exchange rate constant, $\tau_{CA} = 1/k_{CA}$. Since $\Delta\omega_{CA}$ increases with magnetic field strength, the overall relationship between $\Delta\omega_{CA}$ and τ_{CA} will be a function of the field strength of the MR experiment. Because the exchange rate is often highly sensitive to proton concentrations (*13, 14*), pH will be an important factor in determining the effectiveness of an agent. In addition, it is important to realize that temperature (*10*) and the ionic environment (*13*) can also influence the chemical exchange rate.

Chemical Shift

A large chemical shift between water and its proton exchange site on a candidate agent is advantageous for this approach. According to Eq. [3], the larger the chemical shift between water and the agent, the greater the exchange rate can be without approaching the fast exchange limit. The higher chemical exchange rate results in a larger CEST (Eq. [1]).

The larger $\Delta\omega_{CA}$ also improves the specificity of the CEST effect. The magnetic field inhomogeneity for many tissues can exceed 2 ppm (*8*). Thus, a chemical shift beyond 2 ppm is desirable to avoid direct irradiation of water in these inhomogeneous regions. A larger $\Delta\omega_{CA}$ will also permit the use of broadband irradiation to achieve saturation of the agent without direct effects on water protons. This is advantageous to avoid magnetic susceptibility resulting in poor agent saturation due to magnetic field variations.

An additional advantage of a large $\Delta\omega_{CA}$ is a reduction in the macromolecular-water MT background. The further away from the water resonance the saturation pulse is applied, the less magnetization transfer between macromolecules and water protons will be observed for a given irradiation power, due to reduced macromolecule saturation (*7, 8*).

In this preliminary study, we are interested in establishing the classes of exchange sites and compounds that might be useful in the CEST approach. Thus, issues of osmolality, solubility, specificity, and toxicity of the compounds were not evaluated, but will be critical for any final implementation of this approach. Based on the above considerations we searched for compounds with proton chemical exchange sites with large observed chemical shifts, high solubility, and appropriate chemical exchange rates at pH 7.4 and T = 37°C.

MATERIALS AND METHODS

Test solutes were dissolved in HPLC grade water with inorganic phosphate buffers (*14*) to maintain pH. All chemicals were obtained from commercial sources (Aldrich Chemical Co., Milwaukee, WI; Mallinckrodt Specialty Chemical Co., Paris, KY; and Sigma Chemical Co., St. Louis, MO). Phosphate buffer concentration affected CEST results (*13*) and was held constant at 20 mM except as noted. Screening studies were performed at 7 T where saturation transfer spectra were acquired using a Bruker AC-300 wide-bore spectrometer maintained at 37 ± 0.1°C (except as noted) with heated N_2.

The spectral dependence of the CEST effects was determined by sweeping the irradiation frequency and monitoring the effects on the water resonance. Studies were conducted using a steady-state irradiation (15 s, $>3\ T_1$) over a range of frequencies ±8 ppm from water. The observation frequency was set on the water peak and the decoupler used to provide off-resonance saturation. The M_S data were plotted in the form of water amplitude versus irradiation frequency for a constant power level. This action spectrum of irradiation effects as a

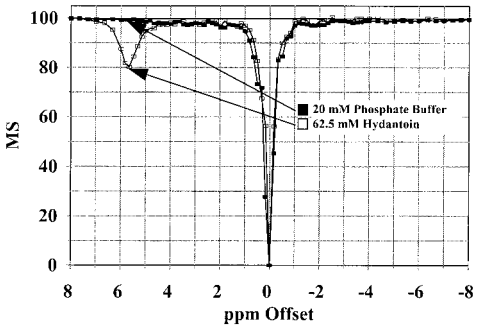

FIG. 1. Representative chemical exchange dependent saturation transfer (CEST) spectra of phosphate buffer (20 mM, pH 4.0) and hydantoin (62.5 mM, 20 mM phosphate buffer, pH 4.0) solutions at T = 37°C.

function of frequency offset is termed a CEST spectrum. A single-acquisition FID was collected following each off- resonance saturation with the following pulse sequence parameters: 90° flip angle, 8192 data points, resolution of 0.977 Hz/pt, acquisition bandwidth = 8000 Hz. The M_S amplitudes were obtained following postprocessing (baseline correction, line broadening (5 Hz), and phase correction) of the individual free-induction decays.

Spin–lattice relaxation time constants (T_1) were obtained with inversion-recovery experiments. The range of inversion delays (T_i) was between 0.001 and 30 s, with a 30-s predelay. A four-acquisition FID was collected for each inversion delay using the above pulse sequence parameters and postprocessing. Similar inversion recovery experiments were conducted to measure the T_1 in the presence of metabolite saturation (T_{1SAT}) in order to estimate the pseudo first-order rate constant, k_1, from Eq. [1]. In these experiments the magnetization was prepared with a 30-s off-resonance irradiation before beginning the inversion-recovery portion of the experiment. After the 180° pulse the irradiation was again applied to maintain the spin saturation during the inversion-recovery time. After post-processing, the water peak amplitudes were fitted to a single exponential to determine either T_1 or T_{1SAT}.

Imaging studies were collected on a 4-T Oxford magnet (T ~25°C for phantom experiment). See figure legends for parameters.

RESULTS

Figure 1 is an example of CEST spectra from solutions of hydantoin (62.5 mM, 20 mM phosphate buffer) and phosphate buffer (20 mM). The magnitude of the water proton signal with presaturation (M_S) is plotted versus the frequency offset of the saturation pulse at constant power. Preirradiation at the water resonance (0 ppm) reduced M_S to ~0 in both samples. However, in the hydantoin solution a second CEST spectral peak at +5.67 ppm was observed that caused a ~20% drop in water signal due to proton chemical exchange at the 3 –NH site on this heterocyclic ring chemical.

Using this type of spectral data, we determined the optimal CEST spectral response for each compound evaluated. This optimum was defined, for a specific concentration and saturation power, as the smallest observed M_S/M_O value (M_O is the magnitude of the signal under control irradiation at the opposite frequency offset from water) for an exchange site. Because the CEST response changes as a function of pH, each compound was evaluated over a range of pH values. Generally, the results at the optimal pH are reported. For each compound, Table 1 lists proton exchange functional group, associated optimum CEST offset frequency ($\Delta\omega_{OBS}$ in ppm), pH, minimum M_S/M_O, concentrations studied, and corresponding maximum ($M_O - M_S$).

Several classes of chemical exchange sites were evaluated. Sugar hydroxyl groups provided good chemical exchange sites at pH 7 ($M_S/M_O = 0.89-0.68$; 250 mM sugar) but their $\Delta\omega_{OBS}$ values (<2 ppm) were too small for *in vivo* use. Sugar polymers, such as dextran, maintained these chemical exchange and shift properties but provided numerous exchange sites per osmole. This result demonstrated the use of polymerization as a method to increase the number of sites without a large accompanying osmotic load.

Backbone amino acid amino and the arginine R group, guanidinium, protons provided a better contrast agent model with $\Delta\omega_{OBS}$ of 2–3 ppm. These compounds, however, were in fast exchange at pH 7.0.

We evaluated additional ring –NH groups present on imino acids, indoles, nucleosides, and their pyrimidine and purine bases, as well as those on derivatives of barbituric acid and imidazole. Several of these compounds revealed promising properties with $\Delta\omega_{OBS}$ >3.0 ppm and M_S/M_O values in the range of 0.7 (62.5 mM). Analyses of these chemicals also demonstrated how pH, phosphate concentration (*13*), and temperature affect CEST results.

Shifts in pH affect k_{CA} because H^+ and OH^- are reactants contributing to the overall proton exchange rate. The effects of pH are readily observed in the CEST spectrum of 5,6-dihydrouracil (Fig. 2A). This compound possesses two base-catalyzed exchange sites with different chemical shifts at 5.00 and 2.67 ppm. The proton exchange rate dependence on pH is different at the two sites. At pH 5.0, the 2.67-ppm site is in very slow exchange resulting in almost no CEST effect, while the 5.00-ppm site is somewhat faster causing a CEST peak to be observed. At pH 6.0, the 2.67-ppm site is now observed in the CEST spectrum while the effect at 5.00 ppm has increased. At pH 7.0, the 2.67-ppm site has increased while the 5.00-ppm peak has apparently entered the intermediate exchange rate resulting in a shift in the optimum toward the larger water pool resonance and a broadening of the CEST spectrum.

Because of the above pH effects, a 20 mM phosphate concentration standard was selected to ensure a stable pH for test solutions across a range of temperatures. Any changes in phosphate concentration may result in CEST spectral differences due to potential catalytic effects of phosphate (*13*). To

TABLE 1
Chemical-Exchange-Dependent Saturation Transfer Data from All Compounds Evaluated in this Study

Compound[a]	Conc (mM)	Functional group	ppm[b]	pH[c]	M_S/M_O	$M_O - M_S$ (%)
Sugars[d]		Hydroxyl protons (–OH)				
Mannitol	250 mM	–OH	1.000	7.0	0.89	9.0
Sorbitol	250 mM	–OH	1.000	7.0	0.88	7.3
Fructose	250 mM	–OH	1.333	7.0	0.88	9.3
Dextrose	250 mM	–OH	1.500	7.0	0.89	8.7
Galactose	250 mM	–OH	1.167	7.0	0.85	10.3
Sucrose	250 mM	–OH	1.333	7.0	0.86	10.2
Maltose	250 mM	–OH	1.500	7.0	0.79	14.8
Lactose	250 mM	–OH	1.333	7.0	0.68	20.9
Dextran[e]						
1.75 gm/100 ml	0.25 mM	–OH	1.167	7.0	0.91	8.1
3.50 gm/100 ml	0.5 mM	–OH	1.333	7.0	0.88	10.2
7.00 gm/100 ml	1.0 mM	–OH	1.333	7.0	0.81	13.6
14.0 gm/100 ml	2.0 mM	–OH	1.500	7.0	0.76	18.9
Amino acids[f]		Amino protons ($–NH_2$)				
L-Alanine	125 mM	$–NH_2$	3.000	4.0	0.36	67.4
L-Arginine	125 mM	$–NH_2$	3.000	4.0	0.36	65.8
L-Arginine	125 mM	Guanidinium protons	2.000	5.0	0.33	57.7
L-Lysine	125 mM	$–NH_2$	3.000	4.0	0.34	66.2
L-Glutamine[g]	125 mM	$–NH_2$	2.000	5.2	0.70	27.6
L-Tryptophan[g]	35 mM	$–NH_2$	2.000	6.5	0.89	12.2
5-Hydroxytryptophan[h]	62.5 mM	$–NH_2$	2.833	4.0	0.57	41.6
		Indole ring –NH	5.333	8.0	0.79	21.2
Nucleosides and their pyrimidine and purine bases[h]		Base protons (–NH)				
5,6-Dihydrouracil	62.5 mM	3-NH	5.000	6.0	0.78	22.2
5,6-Dihydrouracil	62.5 mM	2-NH	2.667	7.0	0.77	22.2
Uridine[i]	125 mM	3-NH	6.333	4.0	0.65	34.7
Thymidine[i]	125 mM	3-NH	6.333	5.0	0.65	34.8
Barbituric acid and its derivatives		Pyrimidine ring protons (–NH)				
Barbituric acid[h]	62.5 mM	–NH	5.000	6.5	0.68	32.5
2-Thiobarbituric acid[h]	62.5 mM	–NH	6.333	5.0	0.65	35.3
5-Isopropylbarbituric acid)[h]	62.5 mM	–NH	5.000	7.0	0.64	36.0
Barbital (5,5-diethyl-barbituric acid)[h]	62.5 mM	–NH	5.000	4.0	0.82	14.2
Imino acids (their azetidine, pyrrolidine, and piperidine forms)		Base protons (–NH)				
Pipecolinic acid[f]	62.5 mM	–NH	3.33	5.0	0.81	19.3
4-trans-Hydroxyproline[f]	62.5 mM	–NH	4.50	4.0	0.77	18.6
		–NH	3.50	4.0	0.80	20.0
Azetidine-2-carboxylic acid[f]	62.5 mM	–NH	3.50	5.0	0.74	25.5
Miscellaneous						
Guanidine HCl[d]	125 mM	Guanidinium protons	2.000	7.0	0.38	60.0
Hydantoin[f]	62.5 mM	–NH	5.667	4.0	0.81	18.7
		–NH	2.833	6.0	0.78	21.3
Parabanic acid[f]	62.5 mM	–NH	5.167	7.0	0.79	20.5
		–NH	3.333	8.0	0.74	25.4
		–NH	2.333	8.0	0.77	22.5
Imidazole and its derivatives:						
2-Imidazolidone[f]	62.5 mM	Ring protons (–NH)	1.167	5.0	0.68	30.4
		Ring protons (–NH)	1.167	8.0	0.68	29.8
2-Imidazolidinethione[f]	62.5 mM	Ring protons (–NH)	2.833	3.0	0.64	36.7
		Ring protons (–NH)	2.833	7.0	0.65	34.5

[a] All compounds were evaluated at 37°C and were dissolved in HPLC water using a 20 mM phosphate buffer unless otherwise noted.
[b] Ppm listed is relative to the resonant frequency of water.
[c] The pH listed is where the greatest proton chemical exchange effect was noted, save for those solutions only evaluated at pH 7.
[d] These compounds were evaluated at a single pH level of 7.0.
[e] Dextran molecular weight was approximately 70,000 gm/mol; thus, concentrations listed (mM) for these solutions are approximate.
[f] All solutions were evaluated at pH 4, 5, 6, 7, and 8, except for L-glutamine and L-tryptophan.
[g] Solution was evaluated at 25°C.
[h] These solutions were evaluated at pH 4, 5, 6, 7, and 8. 5,6-Dihydrouracil, 5-hydroxytryptophan, and barbituric acid solutions were also evaluated at pH 6.5 and 7.4.
[i] All solutions of this compound were evaluated using a 2 mM phosphate buffer. Because phosphate is the optimal physiologic catalyst of proton chemical exchange (*13*), the use of a 20 mM concentration increased the exchange rate observed, increased the desired exchange M_S/M_O ratio, and decreased the ($M_O - M_S$).

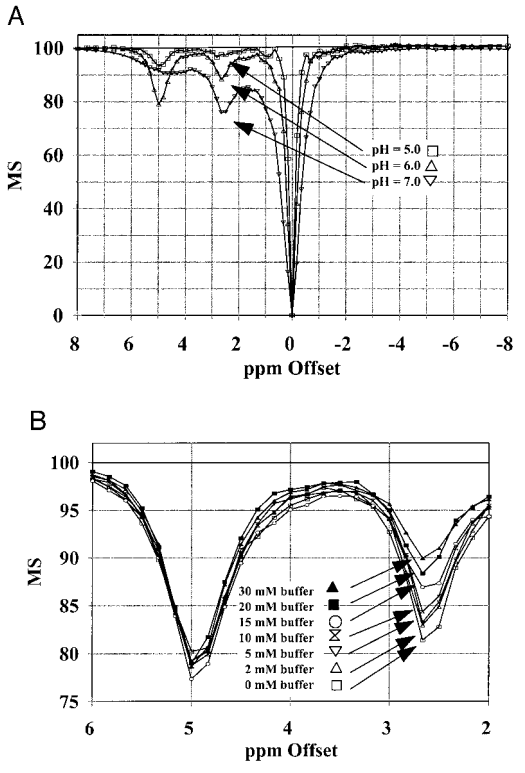

FIG. 2. (A) CEST spectra of 5,6-dihydrouracil (62.5 mM, T = 37°C, 20 mM phosphate buffer, pH 5.0, 6.0, 7.0). Two exchange sites are noted at 5.00 and 2.67 ppm. (B) CEST spectra from 5,6-dihydrouracil solutions evaluated with varying levels of phosphate buffer at constant pH (62.5 mM, T = 37°C, pH 6.0).

test the effect of phosphate on the CEST spectra, the buffer concentration was varied from 0 to 30 mM in a 5,6-dihydrouracil solution (Fig. 2B). Changes in phosphate buffer concentration affected only the 2.67-ppm exchange site and reduced its apparent rate with increasing buffer concentration. The mechanism of this inhibitory effect of phosphate is unknown, but the data demonstrate that phosphate, or other catalytic compounds, can significantly affect the chemical exchange rate. In addition, these results reveal that this effect can even differ between exchange sites present on the same molecule. Increased solution temperature increases most chemical exchange rates as illustrated by the barbituric acid CEST spectrum (Fig. 3). The increase in temperature from 25 to 37°C changed the CEST optimum at 5.00 ppm from slow to intermediate exchange. The above results also underscore the importance of controlling pH and phosphate (and potentially other proton buffers) concentration, as well as temperature in evaluating CEST effects. The phosphate dependence of CEST may provide a new method of detecting phosphate.

Remaining experimental results further characterize another prototypical CEST compound, barbituric acid. This compound was selected because it combined a chemical exchange site at 5.00 ppm with a maximal CEST effect at pH 6.5. It was also selected because it has a low oral toxicity (LD50 $>$ 5000 mg/kg, Sprague–Dawley adult rats; LD50 = 5124 mg/kg, 1-day-old Charles River rats (*15*)).

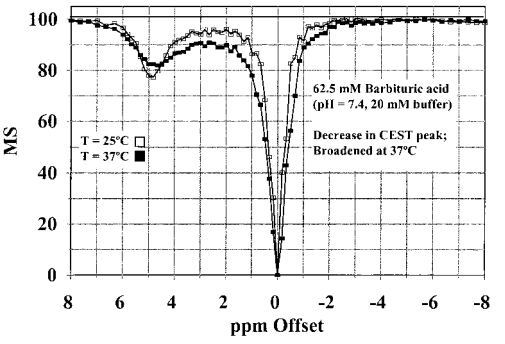

FIG. 3. Temperature-dependent CEST spectra of barbituric acid solution (62.5 mM, 20 mM phosphate buffer), pH 7.4.

The saturation of a chemical exchange site is both a power- and an offset frequency-dependent phenomenon. Individual CEST spectra only present the frequency-dependent component. Because the maximum M_S/M_O effect only occurs when the exchange site is maintained in the completely saturated state, it is crucial to optimize to an appropriate B_1 power level while evaluating compounds in solution. As shown in Fig. 4, the observed ($M_O - M_S$) increases with increasing power, until complete saturation of the barbituric acid exchange site is attained ($\sim B_1 = 25.8 \times 10^{-7}$ T). Due to the differences in T_2 associated with the exchange rate, power requirements differed between exchange sites depending on experimental conditions and were calibrated for each experiment.

Figure 5 presents the effects of pH on barbituric acid at 37°C (Fig. 5A, pH 6.0 to 8.0; Fig. 5B, pH 7.0 to 8.0). The barbituric acid exchange site at ~4.83 ppm is in near fast exchange at pH 8.0 but slows with decreasing pH to a sharp CEST peak at pH 6.5 with the optimum at 5.0 ppm. The compound exhibits a significant 15% $M_O - M_S$ effect under physiologic conditions (pH 7.4, T = 37°C, 20 mM phosphate buffer). Since both protons on water contribute to the overall water signal ampli-

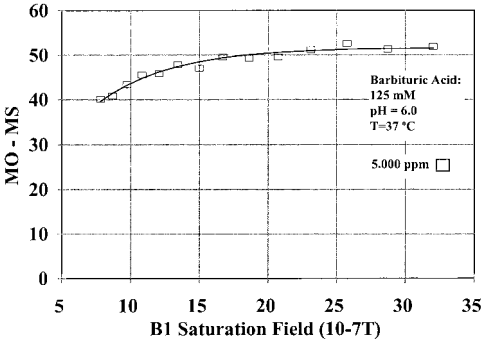

FIG. 4. Power dependence of CEST spectral maxima ($M_O - M_S$) versus increasing B_1 saturation pulses for barbituric acid (125.0 mM, T = 37°C, 20 mM phosphate buffer, pH 6.0).

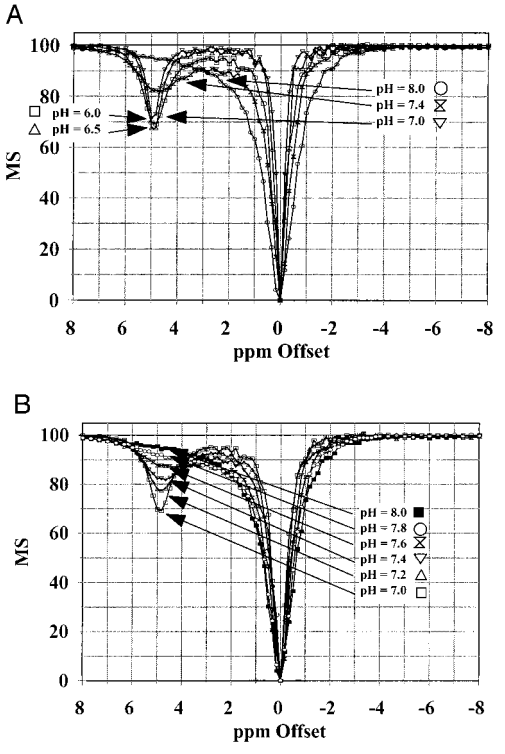

FIG. 5. (A) CEST spectra of barbituric acid (62.5 mM, T = 37°C, 20 mM phosphate buffer, pH 6.0, 6.5, 7.0, 7.4, 8.0). (B) CEST spectra of barbituric acid demonstrating the effect of small incremental changes in pH (62.5 mM, T = 37°C, 20 mM phosphate buffer, pH 7.0, 7.2, 7.4, 7.6, 7.8, 8.0).

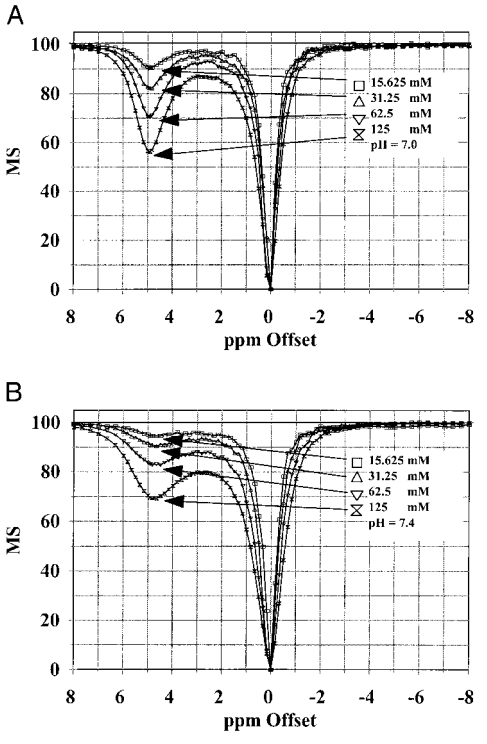

FIG. 6. CEST spectra of barbituric acid solutions at varying concentration levels using a B_1 field of 10.88×10^{-7} T (T = 37°C, 20 mM phosphate buffer) (A) pH 7.0 (B) pH 7.4.

tude and each proton is equally likely to participate in proton chemical exchange with the metabolite compound, this effect is equivalent to an ~16.5 M decrease in the water proton concentration from ~110 M (2 × 55 M, molecular water concentration). Thus, CEST provides an effective amplification of 26,400% (16.5 M/62.5 mM × 100%) of the 62.5 mM barbituric acid under these conditions. These results are consistent with those obtained from imaging experiments previously reported, where a solution of ammonium chloride (62.5 mM, pH 5.0, T = 23°C) provided an $M_O - M_S$ of 50% and an amplification of 88,000% (55 M/62.5 mM × 100%) (*6*).

Figures 6A and 6B demonstrate the concentration dependence of barbituric acid on the CEST effect at two values of pH. The CEST effect linearly increased with [barbituric acid] at both pH values. Note that, despite the increase in rate, the lineshape of each set of curves is maintained, regardless of concentration. This is consistent with the barbituric acid exchange site rate constant (k_{CA}) being unaffected by changes in the mole fraction of exchange sites. These results are also consistent with enhancement of the CEST effect through increases in mole fraction of exchange sites as outlined in Eq. [2].

The pseudo first-order rate constant (k_1) was determined for barbituric acid at pH 6.0, where the compound remains in slow exchange, as evidenced by the sharp spectral peak in Fig. 5A. Experiments similar to those presented in Figs. 6A and 6B were carried out along with corresponding inversion-recovery experiments to determine T_{1SAT} of the same samples. Using Eq. [1], k_1 was calculated for each sample and is clearly linear with barbituric acid concentration (Fig. 7), with a slope of 2.158/M/s.

An imaging series of barbiturate-containing phantoms is presented in Figs. 8A and 8B. Three of the test tube phantoms in this image contain 62.5 mM barbituric acid (pH 6.5, 7.0, and 7.4). The fourth test tube contains 500 mM NH_4Cl at pH 5.0 as another chemical exchange site for control.

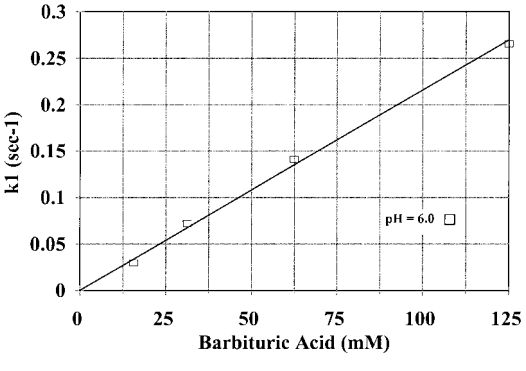

FIG. 7. Pseudo first-order rate constant (k_1) determination plotted versus barbituric acid concentration (T = 37°C, 20 mM phosphate buffer, pH 6.0).

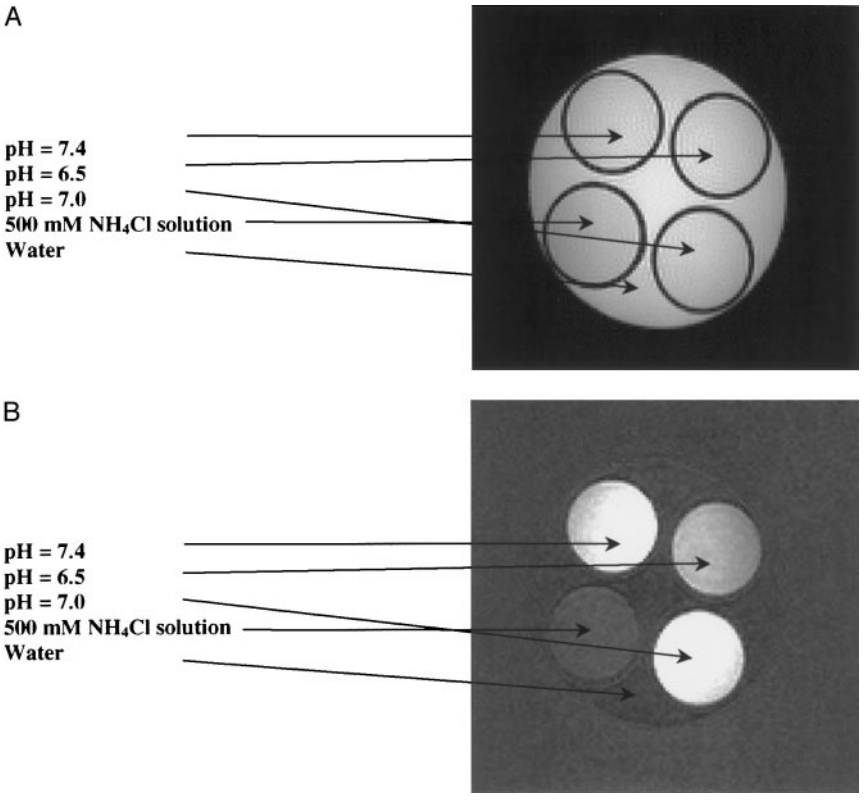

FIG. 8. (A) Image obtained at 4 T of barbituric acid solutions (62.5 mM, ambient temperature ~20°C, 20 mM phosphate buffer, pH 6.5, 7.0, 7.4) and NH_4Cl (500 mM, pH 5.0, no buffer) submerged in water following irradiation at −900 Hz. (B) Difference image obtained of the same phantoms following irradiation at ±900 Hz. NH_4Cl was used as a control proton chemical exchange agent to test the specificity of the CEST effect.

These test tubes were placed inside the 4-T custom imaging system (ambient temperature ~25°C). Figure 8A is the control image obtained after irradiation at −900 Hz. The phantoms were then irradiated at +900 Hz (~5 ppm, based on Fig. 5A data) to detect barbituric acid (see (*6*)). Figure 8B is the difference image generated by subtraction of the +900-Hz (experimental) image from the −900-Hz (control) image. All three solutions of barbituric acid (pH 6.5, 7.0, and 7.4) were enhanced while neither the surrounding water nor the NH_4Cl controls were significantly affected. The brightest signal in these phantoms (where the control and experimental image difference was the greatest) was generated by barbituric acid at pH 7.0. The experimental results presented in Fig. 5A would have predicted that the greatest contrast, as indicated by $(M_O - M_S)$, should have been observed from the pH 6.5 solution. However, because the ambient temperature of the 4-T system was significantly lower than 37°C, subsequent studies were conducted at 25°C on the 7-T system (Fig. 3; additional data not shown). The results demonstrated that temperature-specific shifts in the proton chemical exchange rates produced $(M_O - M_S)$ results at 25°C consistent with the contrast effects observed in Fig. 8C.

DISCUSSION

The potential advantages of a CEST agent when compared with currently available contrast agents are the ability to turn the contrast effect off and on, a negative contrast, no T_2^* effects, ability to enter cells, and potentially less toxicity. The CEST effect can be turned off either by eliminating the preirradiation step or by changing its frequency; thus images can be interleaved with and without contrast agent effects. This might be useful in evaluating different pathologies as well as specificity of the agent. The negative contrast might be useful in the elimination of bright signals, such as blood, in T_1-weighted sequences. A drawback of this negative contrast, however, is that tissue not affected by the CEST contrast agent cannot be suppressed in the image as is done with T_1 contrast agents. This may limit the contrast to noise in a single image obtained through this approach. To get similar contrast to noise with CEST agents, two interleaved images will be required, one with and one without the CEST effect. An alternative imaging strategy would eliminate the need for the control image, but would provide contrast at the expense of diminished M_Z due to saturation transfer. First, an inversion-recovery pulse sequence is adjusted for an inversion time in the absence of off-resonance irradiation. When the irradiation pulse is turned on, the

pulse sequence will highlight areas of the tissue where water is in exchange with the CEST agent. These areas appear with a positive contrast because the irradiation pulse shortens their observed T_1 (T_{1SAT}).

As previously mentioned, magnetization transfer techniques currently exploit the contrast that can be generated from interactions between macromolecules and water protons. MT imaging sequences normally use a single off-resonance saturating pulse to prepare the magnetization before the imaging data are collected. Because CEST contrast is gained via a similar off-resonance saturating pulse, an appropriate imaging scheme is required to produce contrast specifically attributable to a CEST contrast agent alone. Initial proton chemical exchange imaging work (*6*) utilized a scheme where two images were collected: the first following irradiation at the metabolite site of interest (M_S image) and the second following the irradiation of the opposite side of the water resonance from the site of interest (M_O image). Pixel-by-pixel division (M_S/M_O) or subtraction ($M_O - M_S$) of the images produced a final image with contrast due to the proton chemical exchange agent. The usefulness of this approach was further demonstrated in experiments using a proton chemical exchange model system consisting of ammonia (metabolite) in 3% agarose gel (macromolecular matrix) (*8*). The results indicated that the simple control imaging approach was also sufficient to substantially eliminate the MT contribution of the background macromolecular matrix. The approach worked because the magnetization transfer spectrum of the agarose gel was symmetric around the water resonance, as were the MT spectra of most of the biological samples examined under similar experimental conditions. It proved effective to detect an ammonia concentration of 10 mM against a background macromolecular M_S of ~62% at ~2.4 ppm in the model system. The control irradiation imaging approach was, therefore, implemented for the imaging portion of this preliminary CEST contrast agent study.

A major practical issue for future applications of the CEST contrast agent approach concerns *in vivo* agent concentration. Since no metal is needed in the CEST agents, no T_2^* effects will be induced at high contrast agent doses. Agent dosage would be limited only by the physiologic toxicity of the final formulation. The more crucial question is the lower bound on agent concentration to ensure reliable CEST image contrast. The minimum lifetime of a proton on a CEST molecule (τ_{CA}) can be estimated at 1.5 T to be ~5 ms assuming a 5-ppm chemical shift and a $\tau_{CA}\Delta\omega_{CA} = 10$. Assuming a T_1 (in the absence of exchange) of 1.5 s in blood and a useful M_S/M_O of 0.9, the pseudo first-order rate constant, k_1, would be ~0.07 s^{-1} (*9*). To attain this rate constant, the mole fraction of the CEST agent protons relative to water protons must then be on the order of 3.5×10^{-4} or a concentration of 39 mM. This calculation also underscores the importance of having multiple exchange sites per molecule to reduce the osmotic load of the CEST agent.

As previously outlined, an ideal CEST contrast agent would possess the following combination of characteristics. It would have a rapid exchange rate at physiologic temperature and pH but one that remains below the slow to intermediate exchange rate limit relative to $\Delta\omega_{CA}$ (Eq. [3]). An ideal agent would also possess a large $\Delta\omega_{CA}$ to support this rapid k_{CA} and thus maintain a correspondingly minimal M_S/M_O. In addition, a high $\Delta\omega_{CA}$ would enhance specificity, avoid direct irradiation of water resonance, allow use of a broadband pulse, and reduce background macromolecular-water magnetization transfer effects. The ideal agent would also be highly water soluble with low osmolality and biochemical toxicity.

We began this study with a small group of preliminary CEST candidates chosen primarily because their frequency offsets were at or greater than 2 ppm from water (amino acids; (*14*)). No advance knowledge of pH, temperature, or buffer-specific CEST effects was available. Follow-on compounds were chosen because their offset was at or greater than 5 ppm from the water resonance (pyrimidine bases; (*14*)). While these chemicals did possess a more advantageous offset, optimal CEST results remained outside the desired physiologic pH range. Solubility problems limited initial analysis of L-tryptophan, but the large chemical shift offset of the labile indole ring proton (*14*) might be promising for future modifications. 5-Hydroxytryptophan, a more soluble derivative, clearly possessed the same proton chemical exchange site as L-tryptophan with a large frequency shift (5.33 ppm) combined with a useful exchange rate at pH 7.4. Regrettably, 5-hydroxytophan is a neuronal toxin; however, its exchange site remains the most viable candidate structure identified for further developmental work.

Another ring chemical, imidazolidone, suggested that symmetry of chemical structure could result in two CEST M_S/M_O minima, the second at a physiologic pH level. This observation led to evaluation of barbituric acid, which has a similar ring structure as the previously tested pyrimidine bases, but possesses two identical proton chemical exchange sites. It has the additional advantage of low oral toxicity and was selected, rather than 5-hydroxytryptophan, for further characterization and use in the preliminary imaging studies.

Table 1 contains the optimal CEST data from chemicals selected for this study, the majority of which are heterocyclic ring bases. Several of the chemicals also provide empirical evidence as to features which could alter the optimal pH range of a particular parent molecule, shift its frequency offset, or lessen the problem of osmotic load.

From some systematic studies in the ring molecules, we found that we could shift the shielding and $\Delta\omega_{OBS}$. For example, the replacement of oxygen by sulfur at the C-2 site on barbituric acid caused a +1.33-ppm shift in the –NH site. However, these shielding effects were also accompanied by changes in the optimum pH of the CEST effect. Again, the sulfur replacement caused a drop of 1.5 pH units in the optimal CEST effect. These examples show that the shielding and pH dependence of the exchange rate are often linked through poorly defined mechanisms. A better theoretical model or

extensive empirical survey may result in more ideal CEST agents.

The data acquired from the dextran (glucose polymer) solutions compared those from the various sugar solutions indicate that polymerization may be a primary strategy to lessen or eliminate problems of *in vivo* osmotic load while maintaining the overall magnitude of the CEST effect. However, the polymerization of the heterocyclic compounds identified above may result in detrimental shifts in $\Delta\omega_{OBS}$ and effective pH range, similar to those discussed above.

This preliminary study demonstrates the feasibility of a CEST-based MRI contrast agent. The range of chemicals tested also demonstrates features and strategies that should prove useful to direct future developmental efforts. We would suggest that the most viable candidate structure evaluated here, the single indole ring proton (i.e., 5-hydroxytryptophan), might provide an appropriate starting point for further investigations of potential CEST contrast agents. Other heterocyclic chemicals, such as barbituric acid, may be additional candidates for development, dependent upon the proposed functionality of the final agent.

REFERENCES

1. C. Casali, M. Janier, E. Canet, J. F. Obadia, S. Benderbous, C. Corot, and D. Revel, Evaluation of Gd-DOTA-labeled dextran polymer as an intravascular MR contrast agent for myocardial perfusion, *Acad. Radiol.* **5**(Suppl. 1), S214–S218 (1998).
2. T. Liebig, C. Stoupis, P. R. Ros, J. R. Ballinger, and R. W. Briggs, A potentially artifact-free oral contrast agent for gastrointestinal MRI, *Magn. Reson. Med.* **30,** 646–649 (1993).
3. S. Aime, R. Nano, and M. Grandi, A new class of contrast agents for magnetic resonance imaging based on selective reduction of water-T2 by chemical exchange, *Invest. Radiol.* **23**(Suppl. 1), S267–S270 (1988).
4. V. Govindaraju, D. J. Meyerhoff, A. A. Maudsley, M. Vermathen, and M. W. Weiner, Effects of brain membranes on ^{1}H nuclear magnetic resonance signal intensity of ethanol in vitro, *Alcohol. Alcohol.* **32,** 671–681 (1997).
5. D. J. Meyerhoff, W. D. Rooney, T. Tokumitsu, and M. W. Weiner, Evidence of multiple ethanol pools in the brain: An in vivo proton magnetization transfer study, *Alcohol. Clin. Exp. Res.* **20,** 1283–1288 (1996).
6. S. D. Wolff and R. S. Balaban, NMR imaging of labile proton exchange, *J. Magn. Reson.* **86,** 164–169 (1990).
7. S. D. Wolff and R. S. Balaban, Magnetization transfer contrast (MTC) and tissue water proton relaxation in vivo, *Magn. Reson. Med.* **10,** 135–144 (1989).
8. V. Guivel-Scharen, T. Sinnwell, S. D. Wolff, and R. S. Balaban, Detection of proton chemical exchange between metabolites and water in biological tissues, *J. Magn. Reson.* **133,** 36–45 (1998).
9. S. Forsén and R. A. Hoffman, Study of moderately rapid chemical exchange reactions by means of nuclear magnetic double resonance, *J. Chem. Phys.* **39,** 2892–2901 (1963).
10. R. A. Dwek, "Nuclear Magnetic Resonance (N.M.R.) in Biochemistry," London, Oxford Univ. Press (1973).
11. V. V. Kupriyanov, R. S. Balaban, N. V. Lyulina, A. Steinschneider, and V. A. Saks, Combination of ^{31}P-NMR magnetization transfer and radioisotope exchange methods for assessment of an enzyme reaction mechanism: Rate-determining steps of the creatine kinase reaction, *Biochim. Biophys. Acta.* **1020,** 290–304 (1990).
12. J. R. Alger and R. G. Shulman, NMR studies of enzymatic rates in vitro and in vivo by magnetization transfer, *Q. Rev. Biophys.* **17,** 83–124 (1984).
13. E. Liepinsh and G. Otting, Proton exchange rates from amino acid side chains—Implications for image contrast, *Magn. Reson. Med.* **35,** 30–42 (1996).
14. K. Wüthrich, "NMR of Proteins and Nucleic Acids," Wiley–Interscience, New York (1986).
15. E. I. Goldenthal, A compilation of LD50 values in newborn and adult animals, *Toxicol. Appl. Pharmacol.* **18,** 185–207 (1971).